Layer thickness dependence of CPP giant magnetoresistance in individual CoNi/Cu multilayer nanowires grown by electrodeposition

X.-T. Tang,[1] G.-C. Wang,[1] and M. Shima[2]
[1]*Department of Physics, Applied Physics, and Astronomy, Rensselaer Polytechnic Institute, Troy, New York 12180-3590, USA*
[2]*Department of Materials Science and Engineering, Rensselaer Polytechnic Institute, Troy, New York 12180-3590, USA*
(Received 24 December 2006; revised manuscript received 6 February 2007; published 3 April 2007)

Giant magnetoresistance (GMR) effect of CoNi/Cu nanowires grown by electrodeposition using an array of parallel through holes in anodized alumina membranes was studied in the current-perpendicular-to-plane (CPP) geometry as a function of the CoNi and Cu layer thicknesses. The CPP-GMR measurements were carried out by making a point contact with individual nanowires using a metallic plunger tip. In the range of the CoNi layer thickness t_{CoNi}=2–510 nm and that of the Cu layer thickness t_{Cu}=4.2–42 nm, the maximum value of CPP-GMR change observed in the CoNi/Cu nanowires was 23% at room temperature. The variation of the CPP-GMR with t_{CoNi} at fixed t_{Cu} and that with t_{Cu} at fixed t_{CoNi} is discussed in terms of the series-resistor model and the Valet-Fert model for CPP-GMR. The effects of various factors such as superparamagnetism in very thin CoNi layers and dipole-dipole interactions between CoNi layers on the CPP-GMR of CoNi/Cu nanowires are also discussed.

DOI: 10.1103/PhysRevB.75.134404 PACS number(s): 75.47.De, 75.70.Cn, 72.25.Ba, 81.15.Pq

I. INTRODUCTION

Giant magnetoresistance (GMR) effect observed in magnetic multilayer films consisting of alternating magnetic and nonmagnetic layers represents a relatively large change in the electrical resistance when an external magnetic field is applied to the films.[1] The GMR effect was first observed in the current-in-plane (CIP) geometry, which has been used in the read-head components of hard disk drives since 1997.[2] The study of the GMR effect is very important for the development of science and technology for future device applications, and further research efforts have been made to better understand the fundamental mechanism of the spin-transport phenomena. The GMR effect of magnetic multilayers measured in the current-perpendicular-to-plane (CPP) geometry is technologically more advantageous than that in the CIP geometry because the CPP-GMR is usually larger than the CIP-GMR.[3] It is possible to gain insights into the spin-transport mechanism in CPP-GMR by interpreting experimentally obtained GMR data with appropriate theoretical models. The analysis using these theoretical models is expected to help in determining various physical parameters important to explain the spin-transport properties. However, it is technically challenging to measure and characterize the CPP-GMR effect of a conventional multilayer thin film due to its very small resistance across the film because the film thickness is much smaller than its lateral dimensions. Pratt *et al.* has managed to measure the CPP-GMR effect of multilayer films at low temperatures by a complicated method that is based on a superconducting quantum interference device (SQUID).[4] The CPP-GMR effect of magnetic multilayers has also been studied at room temperature in the form of lithographically-patterned pillars,[5,6] films grown on grooved substrates,[7] and electrodeposited nanowires.[8–11] Electrodeposited multilayer nanowires provide an ideal opportunity to investigate the CPP-GMR effect since nanowires with large aspect ratio (length/diameter) can be easily grown. The high aspect ratio of nanowires would ensure much higher electrical resistance than that of thin films so that the CPP-GMR effect can be measured more accurately. Electrodeposited multilayer nanowires can be grown into a pore pattern of templates made of various materials such as anodized alumina and polycarbonate.[8–11]

Although multilayer nanowires are ideal for the study of the CPP-GMR effect as described above, there remains a technical difficulty in making an electrical contact with individual nanowires for the CPP-GMR measurements. When nanowires are made inside the pores of a template, the conventional four-point probe method cannot be simply employed in this geometry. Also, the number of nanowires used for CPP-GMR measurements should be minimized in order to maintain a relatively large electrical resistance. One method to limit the number of nanowires is to coat a thin conducting layer on the top surface of a template so that the growth of the nanowires can be terminated when the first nanowires reach the top conducting surface, which can be monitored as a sudden increase in the deposition current.[12] Then silver epoxy or paste is used to secure a conducting wire from the top surface of the template in order to establish a closed electrical circuit for MR measurements. The use of silver epoxy or paste may hamper subsequent measurements such as structural or chemical composition analysis. There are several other methods such as the conventional four-point probe method[13] and a use of conductive-tip atomic force microscopy (CT-AFM) (Ref. 14) to measure the CPP-GMR effect of multilayer nanowires. In the case of the four-point probe method, an individual multilayer nanowire needs to be placed onto a stage fabricated with four nanoscale electrodes under scanning electron microscopy (SEM) and electrically connected with the electrodes by electron beam lithography.[13] The CT-AFM method is carried out by forming an electrical contact between the conductive AFM tip and multilayer nanowires made in the holes of a template.[14]

Our first tasks in this work were to technically establish an easy and reliable method and to measure the CPP-GMR of multilayer nanowires using this method. To achieve the

tasks, we utilized a spring-loaded metallic plunger tip that has a micron-size round-shaped head to make an electrical contact with CoNi/Cu nanowires electrodeposited in the holes of an alumina template. This simple method enables us to measure the CPP-GMR effect of selected CoNi/Cu nanowires at a desired location on the surface of a template.

Previously reported CPP-GMR data have been mostly interpreted using the series-resistor model[15,16] since it provides a better approximation for the CPP-GMR than the CIP-GMR. The series-resistor model was initially developed using the two-current model proposed by Mott.[17] The Mott model assumes that no spin-flip scattering occurs during the transport of electrons and that the currents through the two different spin channels (spin up and spin down) are described independently. Under these assumptions, the conduction through these spin channels occur in parallel. Lee *et al.* further developed the series-resistor model for the CPP-GMR effect of magnetic multilayers.[18] Lee's model takes into account various parameters that contribute to the CPP-GMR effect. These parameters include the resistivity of nonmagnetic layers, the spin-dependent resistivity of magnetic layers, the spin-dependent interfacial resistance between magnetic and nonmagnetic layers, and the contact resistance by superconducting leads used for the measurement. The series-resistor model is not valid when the spin flipping is not negligible for the CPP-GMR in multilayers.

Valet and Fert[19,20] proposed a different model that modified the series-resistor model and took into account the spin relaxation due to spin-flip scattering in addition to the normal relaxation of electrons associated with momentum. For the steady-state spin transport in a magnetic multilayer, the spin relaxation is balanced with the spin accumulation at the layer interfaces when electrons move in the direction perpendicular to the interfaces. The spin-flip scattering is quantitatively described by the spin-diffusion length. The spin-diffusion length is an important parameter in the Valet-Fert model. When the layer thicknesses are much shorter than the spin-diffusion length, the Valet-Fert model simply represents the same as the series-resistor model.

In this work, CoNi/Cu nanowires with various thicknesses of CoNi and Cu layers were prepared and characterized using a point contact method to gain further insight into the mechanism of the CPP-GMR effect. The obtained data were then interpreted using the series-resistor model and the Valet-Fert model. The effects of various factors such as dipole-dipole interactions between CoNi layers and superparamagnetism in very thin CoNi layers on the CPP-GMR effect in CoNi/Cu nanowires will also be discussed.

II. EXPERIMENTAL

A. Electrodeposition of CoNi/Cu multilayer nanowires

CoNi/Cu multilayer nanowires were grown by electrodeposition using a commercial anodized alumina template (Anodisc®) that has an array of pores with 60 μm in length. According to the supplier of the templates, each 60 μm-long pore consists of two sections A and B in series: section A has several parallel pores with the size of 20 nm in diameter and 1–2 μm in length, and section B has a pore with the size of ~250 nm in diameter and 58–59 μm in length. The detailed information about the template can be found in Ref. 21. The surface of the template ending with section A was coated by 120-nm-thick gold layer using thermal evaporation. This coated surface was used as a working electrode for electrodeposition. The thickness of the gold layer was chosen so that the entire surface area including the open ends of the pores was completely covered with the gold layer. An electrical contact was then made to the gold layer using a conductive tape. The entire area of the gold layer coated side was masked with an insulating tape. Only pores on section B of the template were exposed. The template was then submerged in an electrolytic solution containing 2.3 M $Ni(SO_3NH_2)_2$, 0.4 M $CoSO_4$, 0.025 M $CuSO_4$, and 0.5 M H_3BO_3 at pH 2.2. The Cu^{2+} concentration was kept low so that the rate of reduction for Cu was slow and limited by its diffusion in the solution. Electrodeposition of multilayer nanowires was performed at room temperature using a potentiostat/galvanostat (EG&G Princeton Applied Research Model 273). The electrodeposition cell used for the nanowire growth consists of three vertically-positioned electrodes: a working electrode described above, a counter electrode made of platinum, and an Ag/AgCl reference electrode. The multilayer nanowires were electrodeposited potentiostatically by periodically switching the deposition potential between −0.2 V (vs Ag/AgCl) for Cu layer deposition and −1.0 V (vs Ag/AgCl) for CoNi layer deposition. The thickness of each layer was controlled by monitoring the pulse duration which corresponds to the cumulative charge transferred during the deposition based on Faraday's law of electrolysis. The electrodeposition process was terminated after nanowires grew to the end of the pores in section B of the template.

The structure and the chemical composition of CoNi/Cu nanowires were examined using scanning electron microscopy (SEM), x-ray diffraction (XRD), and wavelength dispersive spectrometry (WDS). After multilayer nanowires were grown, the alumina template was carefully removed from the nanowires by etching it away using 4 M NaOH, and the nanowire structure was examined by SEM. The SEM image shown in Fig. 1(a) clearly demonstrates that the nanowires have a multilayer structure consisting of periodically-alternating CoNi and Cu layers with layer thicknesses $t_{CoNi}=155\pm9$ nm and $t_{Cu}=18\pm3$ nm, respectively. The nanowires have an average diameter of about 250 nm. The XRD data obtained for CoNi/Cu nanowires (not shown here) reveal that the nanowires have a FCC structure with a (111) texture developed in the direction along the nanowires.[22] The compositional analysis of electrodeposited CoNi alloy by WDS has revealed that the composition of the CoNi layers is about $Co:Ni=(56.4\pm5.4):(43.6\pm5.4)$ when the layers are thicker than 10.2 nm.

B. Magnetotransport measurements

The CPP-GMR of CoNi/Cu nanowires was measured using a point-contact method shown in Fig. 1. After nanowires were electrodeposited into pores of a template, the topside of

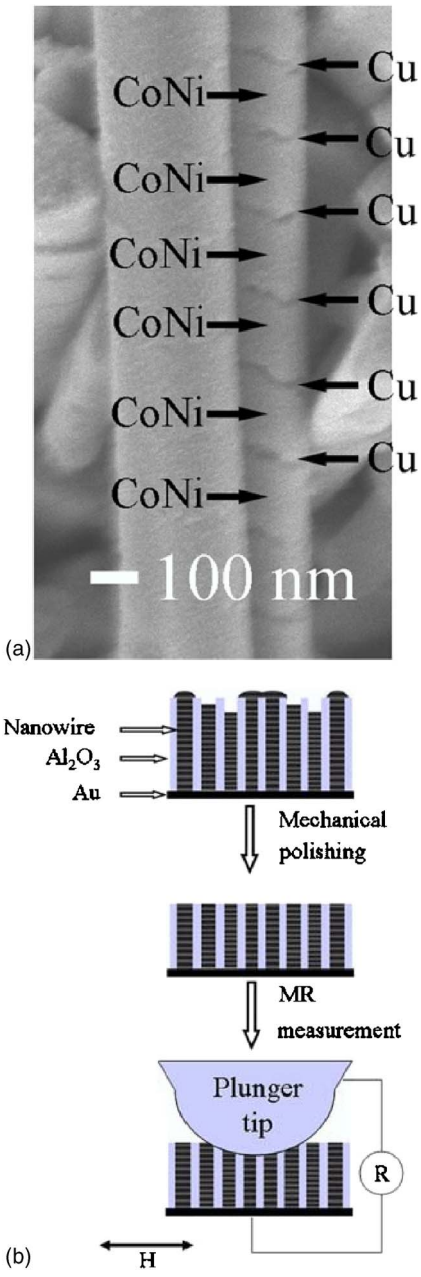

FIG. 1. (Color online) (a) An SEM image of CoNi/Cu nanowires and (b) a schematic representation for the sample preparation process of the multilayer nanowires. The thicknesses of CoNi and Cu layers in the CoNi/Cu nanowires shown in (a) are, respectively, $t_{CoNi}=155\pm9$ nm and $t_{Cu}=18\pm3$ nm. In the sample preparation process, nanowires were first electrodeposited in the pores of an anodized alumina template, and the topside of the template was then mechanically polished using 0.3 μm alumina abrasive particles. The point contact method used for the magnetoresistance measurement employs a plunger tip pressed onto the top surface of the polished sample. The black arrow in (b) represents the direction of an applied magnetic field H.

the 60 μm-thick alumina template was mechanically polished down to approximately 30–40 μm thickness using 0.3-μm alumina abrasive particles. See Fig. 1(b). After the mechanical polishing, a conductive copper tape was electrically connected to the gold coating layer of the template for MR measurements. To make an electrical contact for the MR measurement, a metallic plunger tip was approached to the polished side of the nanowires. The distance between the tip and the sample was manually adjusted using a micrometer with a 2-μm step size. The plunger tip used for this study is a gold-plated high-performance spring-loaded probe (Everett Charles Technologies Model HPA-1B). The tip is spring-loaded on the sample surface to assure its stable contact for MR measurements. After a stable contact was made, magnetotransport measurements were carried out at room temperature under applied magnetic fields up to 9 kOe. The field was applied in the direction perpendicular to the axis of the nanowires. Using this point-contact method, CPP-GMR of selected nanowires at a desired location in the sample can be measured so that it is possible to perform a number of measurements at different locations on the same sample. In contrast, the conventional method to make an electrical contact using a silver epoxy without polishing the topside of the template allows us to measure only the longest nanowires grown all the way to the end of their pores in the template. Hence there are limited locations in the sample available for MR measurements. It is also cumbersome if the silver epoxy needs to be subsequently removed for other measurements.

Typical magnetoresistance (MR) curves measured under various contact conditions using the plunger tip for CoNi/Cu nanowires with $t_{CoNi}=10.2$ nm and $t_{Cu}=4.2$ nm are shown in Fig. 2. R^{AP} and R^{P} are respectively the resistance at the peak position and the resistance at the saturation field of the MR curve, and ΔR is the difference between R^{AP} and R^{P}. The different values of resistance R^{AP} shown in Figs. 2(a)–2(d) were obtained when the value of $\Delta R/R^{P}$ was maximum under conditions when a different number of nanowires were contacted by the plunger tip. It can be readily seen that the measured MR value is nearly independent of the number of contacted nanowires, indicating that the quality and the layer thicknesses of the nanowires are fairly uniform. As shown in Fig. 2(e), the MR values close to 20% are obtained when R^{AP} is in the range 5–95 Ω. When the nanowires having the same resistance are in parallel, the measured value of R^{AP} should be approximately inversely proportional to the number of nanowires. When the contact resistance is negligibly small and all the nanowires are expected to exhibit the same MR change, the net MR change should be independent of the number of nanowires being measured. The MR of a single nanowire is expressed as $MR_{One}=\Delta R_{One}/R_{One}{}^{P}$. Correspondingly, the MR of n numbers of nanowires in parallel is $MR_n=\Delta R_n/R_n{}^{P}=(\Delta R_{One}/n)/(R_{One}{}^{P}/n)=\Delta R_{One}/R_{One}{}^{P}=MR_{One}$. The factor n in the nominator and denominator cancel each other. Therefore the MR is independent of the number of nanowires n being measured.

However, the actual MR changes measured in the nanowires are larger when $R^{AP}\sim20$ Ω than the value obtained for other R^{AP} as shown in Fig. 2(e). To explain the observed variation of MR, it is necessary to take into account the contact resistance arising during the MR measurements. In this case, the MR change can vary with the number of nanowires as shown by the following expressions:

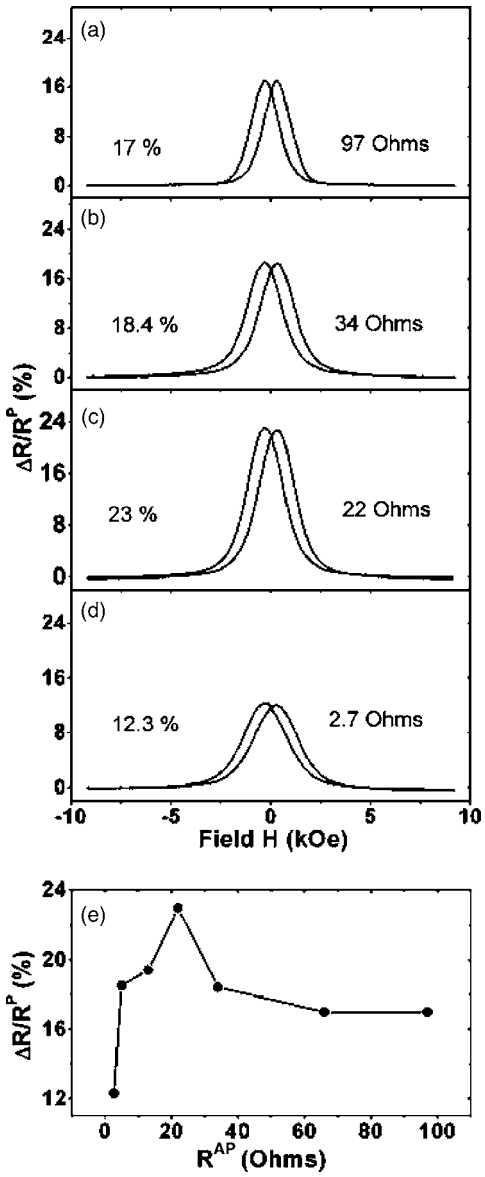

FIG. 2. (a)–(d) Room temperature magnetoresistance (MR) curves measured from CoNi/Cu nanowires with layer thicknesses $t_{\mathrm{CoNi}}=10.2$ nm and $t_{\mathrm{Cu}}=4.2$ nm and (e) the MR changes plotted as a function of the resistance R^{AP} measured in various point contact conditions when the magnetizations of adjacent CoNi layers were aligned antiparallel to each other. The solid curve in (e) is a guide for the eyes.

$$MR_{\mathrm{One}}=\frac{(R^{AP}_{\mathrm{One\ wire}}+R_{\mathrm{One\ contact}})-(R^{P}_{\mathrm{One\ wire}}+R_{\mathrm{One\ contact}})}{R^{P}_{\mathrm{One\ wire}}+R_{\mathrm{One\ contact}}}=\frac{R^{AP}_{\mathrm{One\ wire}}-R^{P}_{\mathrm{One\ wire}}}{R^{P}_{\mathrm{One\ wire}}+R_{\mathrm{One\ contact}}},\tag{1}$$

and

$$MR_{n}=\frac{(R^{AP}_{n\ \mathrm{wire}}+R_{n\ \mathrm{contact}})-(R^{P}_{n\ \mathrm{wire}}+R_{n\ \mathrm{contact}})}{R^{P}_{n\ \mathrm{wire}}+R_{n\ \mathrm{contact}}}=\frac{R^{AP}_{n\ \mathrm{wire}}-R^{P}_{n\ \mathrm{wire}}}{R^{P}_{n\ \mathrm{wire}}+R_{n\ \mathrm{contact}}}.\tag{2}$$

The contact resistance may originate from two possible causes: $R_{n\ \mathrm{contact\ point}}$ from the interface between the plunger tip and the sample, and $R_{n\ \mathrm{contact\ cable}}$ from the bulk resistance of cables and the interface between cables.

$$R_{n\ \mathrm{contact}}=R_{n\ \mathrm{contact\ point}}+R_{n\ \mathrm{contact\ cable}}.\tag{3}$$

When n is large, the resistance of the nanowires decreases and becomes comparable to $R_{n\ \mathrm{contact\ cable}}$ so the MR change is relatively smaller. As n is reduced, the contribution of $R_{n\ \mathrm{contact\ cable}}$ to the overall resistance becomes relatively less significant, the MR changes are larger than those with large n, as shown in Fig. 2. On the other hand, the MR change slightly decreases as n becomes very small. We speculate that the observed variation of the MR change is due to a relatively large contact resistance between the plunger tip and the sample.

It is technically challenging to precisely control the number of contacted nanowires n every time the tip is placed on the sample for a measurement. It is also difficult to determine the number n from the contact area between the tip and the sample. The plunger tip has a semispherical shape of diameter $\sim 80\ \mu$m. The actual contact area between the tip and the sample may be much smaller than the surface area of the tip. In this case, the number n would depend on both the uniformity of the nanowires' length and the actual contact area between the tip and nanowires. Although in principle many nanowires can be in contact with the 80 μm tip, in reality only a small fraction of them were contacted with the tip for MR measurements. Hence, a limited number of nanowires can be measured using the 80 μm diameter plunger tip. Generally no obvious deformation of the tip was observed by optical microscopy after MR measurements however occasionally a partial deformation of the tip was found when it was pressed directly onto an alumina template.

The number of contacted nanowires n can be approximately estimated using the R^{AP} values obtained from MR measurements, the previously-obtained resistivity data for Co and Cu, and the interfacial resistance between Co and Cu layers.[23] Provided that the bulk resistance and the interfacial resistance of CoNi/Cu nanowires are similar to those of Co/Cu nanowires, the estimated resistance of a CoNi/Cu nanowire with $t_{\mathrm{Cu}}=4.2$ nm, $t_{\mathrm{CoNi}}=10.2$ nm, and length 30 μm is $\sim 300\ \Omega$. When the contact resistance is negligibly small, the number of nanowires n estimated from the experimental data shown in Fig. 2(a) is ~ 3 since the value R^{AP} $\sim 97\ \Omega$ is approximately one third of the estimated resistance of a single nanowire. Similarly, $n=\sim 10$, ~ 15, and ~ 100 for the data shown in Figs. 2(b)–2(d), respectively. The actual number of nanowires measured in each case was probably within a few times larger or smaller than these estimated values.

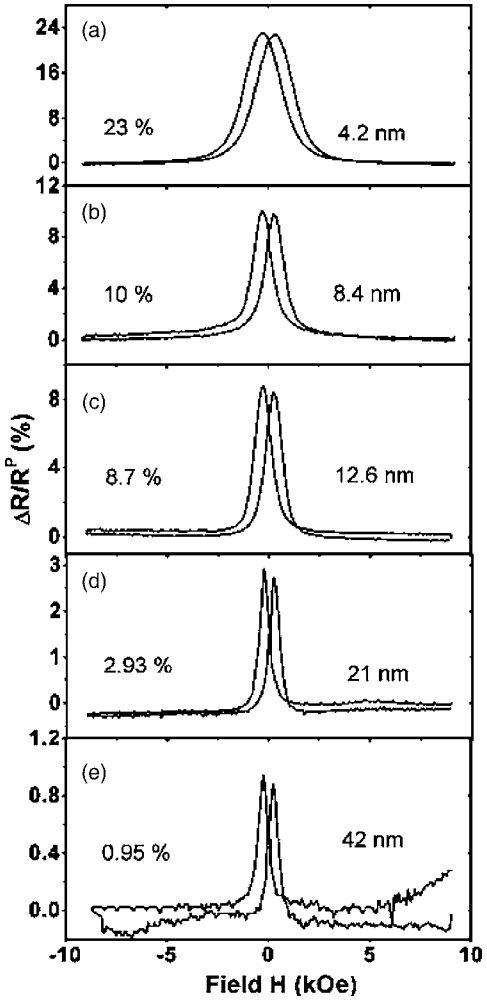

FIG. 3. Room temperature MR curves measured from CoNi/Cu nanowires with layer thicknesses t_{CoNi}=10.2 nm and t_{Cu}=(a) 4.2 nm, (b) 8.4 nm, (c) 12.6 nm, (d) 21 nm, and (e) 42 nm. The value of MR change decreases from 23% to 0.95% as t_{Cu} increases from 4.2 to 42 nm.

III. CPP-GMR RESULTS

The CPP-GMR of CoNi/Cu nanowires was systematically studied as a function of the layer thicknesses. First, the Cu thickness t_{Cu} was varied from 4.2 nm to 42 nm when the CoNi layer thickness t_{CoNi} was fixed at 10.2 nm, and second, t_{CoNi} was varied from 2 nm to 510 nm when t_{Cu} was fixed at 4.2 nm.

A. Cu layer thickness dependence of MR

The magnetoresistance (MR) curves were obtained at room temperature for CoNi/Cu nanowire samples with various Cu layer thicknesses t_{Cu}=4.2 nm, 8.4 nm, 12.6 nm, 21 nm, and 42 nm and fixed CoNi layer thickness t_{CoNi} =10.2 nm. The CPP-GMR curves for selected samples are shown in Fig. 3. As shown in the t_{Cu} dependence of GMR in Fig. 4(a), the MR change decreases with increasing t_{Cu} from 4.2 to 42 nm. The decrease in MR change with increasing t_{Cu} can be explained using the series-resistor model or the

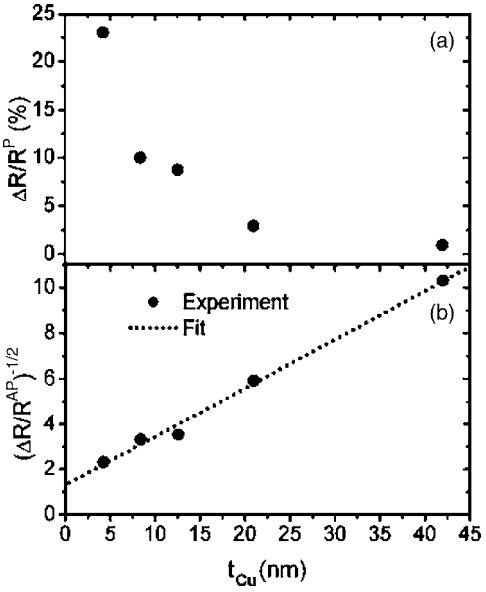

FIG. 4. (a) Room temperature MR changes $\Delta R/R^P$ measured as a function of t_{Cu} for CoNi/Cu nanowires when t_{CoNi}=10.2 nm and (b) the MR changes plotted as a function of t_{Cu}. The values of MR change in (a) are given as $\Delta R/R^P$, and those in (b) are as $(\Delta R/R^{AP})^{-1/2}$. The dotted line was obtained from the Valet-Fert model in the limit of long spin-diffusion length.

Valet-Fert model under the long spin diffusion approximation. It can also be shown that the saturation field determined from the MR curves decreases with increasing t_{Cu}, probably due to a reduced dipole-dipole interaction between neighboring CoNi layers. The effect of interlayer dipole-dipole interaction on the MR curves will be discussed in detail in Sec. IV A.

B. CoNi layer thickness dependence of MR

The magnetoresistance (MR) curves were measured at room temperature for CoNi/Cu nanowire samples with various CoNi layer thicknesses t_{CoNi}=2 nm, 10.2 nm, 17 nm, 34 nm, 51 nm, 102 nm, 170 nm, and 510 nm and a fixed Cu layer thickness t_{Cu}=4.2 nm. The MR of CoNi nanowires without Cu layers was also measured and compared with the data for CoNi/Cu nanowires. Figure 5 shows the CPP-GMR curves for selected samples. As shown in Fig. 6(a), with increasing t_{CoNi} the MR change first increases and reaches a maximum at t_{CoNi}=17 nm and then decreases for t_{CoNi} $>$17 nm. At $t_{CoNi}$$>$510 nm, the MR change does not show much variation with increasing t_{CoNi}. The reduced MR changes for small t_{CoNi} may be due to discontinuity of very thin CoNi layers. The effects of discontinuity in very thin CoNi layers on the MR change will be discussed in detail later. The decrease in MR change with increasing t_{CoNi} from 34 nm to 170 nm can be explained using the Valet-Fert model. The approximately constant MR change for t_{CoNi} $\geqslant$510 nm is probably due to the existence of anisotropy magnetoresistance (AMR).

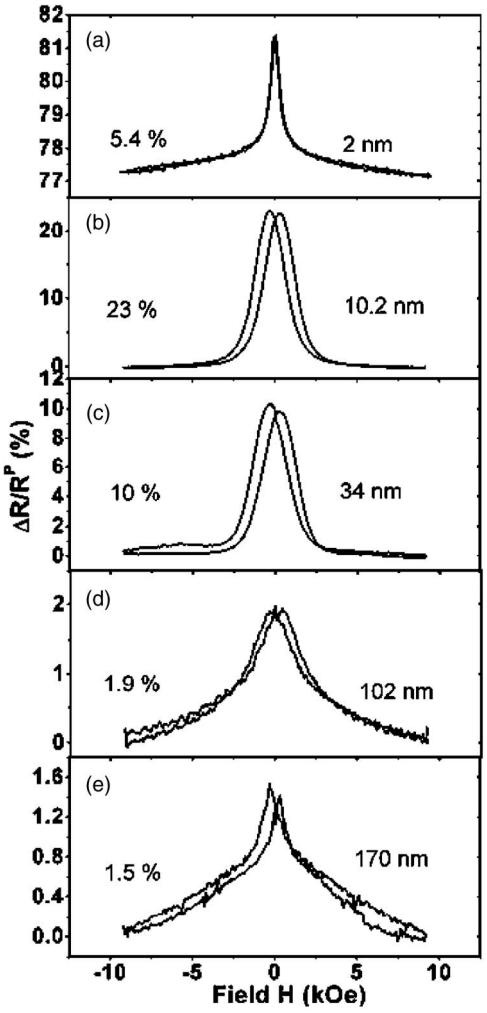

FIG. 5. Room temperature MR curves measured from CoNi/Cu nanowires with t_{Cu}=4.2 nm and t_{CoNi}=(a) 2 nm, (b) 10.2 nm, (c) 34 nm, (d) 102 nm, and (e) 170 nm. With increasing t_{CoNi}, the MR value increases when $t_{CoNi} < 10.2$ nm and decreases when $t_{CoNi} > 10.2$ nm.

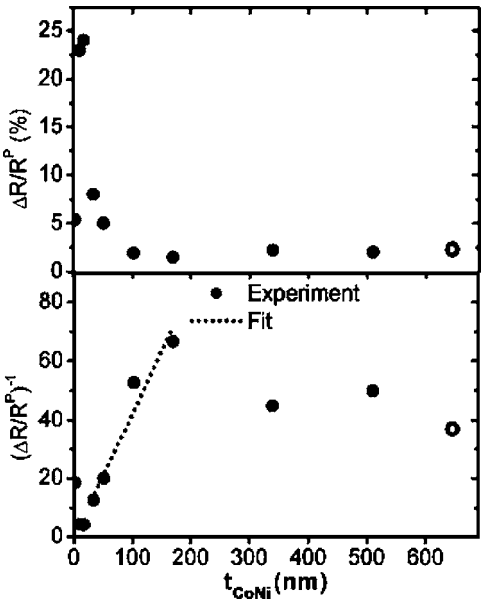

FIG. 6. (a) Room temperature MR changes $\Delta R/R^P$ measured as a function of t_{CoNi} for CoNi/Cu nanowires with t_{Cu}=4.2 nm and (b) the MR changes given as $(\Delta R/R^P)^{-1}$ plotted as a function of t_{CoNi}. The open circles in (a) represent the MR values of monolithic CoNi nanowires with length ~40 μm. The dotted line in (b) was obtained from the Valet-Fert model in the limit of $t_{Cu} \ll l_{Cu}$ and $t_{CoNi} \gg l_{CoNi}$.

IV. DISCUSSION

A. Discussion of parameters in CPP-GMR for CoNi/Cu multilayer nanowires

The experimental data of CPP-GMR obtained for CoNi/Cu multilayer nanowires can be explained using theoretical models such as the series-resistor model[15,16] and the Valet-Fert model.[19,20] The series-resistor model is based on the Mott's two-current model,[17,18] which points out that the electrical conductivity of metals can be described in terms of two independent channels for conduction electrons with up spin and down spin. The net flow of conduction electrons occurs through these channels, and the overall conductivity of a metal is given as the sum of the conductivities of these spin channels. In the series-resistor model each layer or interface is treated as an independent resistor, and the resistors for electrons with each type of spin are summed through the spin channel. In general, the alignment of magnetizations in magnetic layers of a multilayer can be changed by applying a magnetic field, and the resistance of the multilayer varies with the alignment of the magnetizations. According to the series-resistor model, the MR can be described by various parameters including the resistivity ρ_F of the magnetic layer, the bulk spin asymmetry coefficient β, the renormalized resistivity of the magnetic layer $\rho_F{}^* = \rho_F/(1-\beta^2)$, the resistivity of the nonmagnetic layer $\rho_N{}^* (=\rho_N)$, the interfacial spin asymmetry coefficient γ, the renormalized interfacial resistance per unit area $r_b{}^* = r_b/(1-\gamma^2)$, the nonmagnetic layer thickness t_N, and the magnetic layer thickness t_F. The resistivity for the up-spin channel $\rho_\uparrow{}^F$ and that for the down-spin channel $\rho_\downarrow{}^F$ in the magnetic layers are given as

$$\rho_\uparrow^F = 2\rho_F^*[1-\beta], \quad \rho_\downarrow^F = 2\rho_F^*[1+\beta]. \tag{4}$$

In nonmagnetic layers, the resistivity for the up-spin channel is equal to that for the down-spin channel

$$\rho_{\uparrow(\downarrow)}^N = 2\rho_N^*. \tag{5}$$

The interfacial resistivity per unit area for the up-spin channel $r_\uparrow$ and that for the down-spin channel $r_\downarrow$ are expressed as

$$r_\uparrow = 2r_b^*[1-\gamma], \quad r_\downarrow = 2r_b^*[1+\gamma]. \tag{6}$$

When a multilayer with N bilayers (i.e., N pairs of magnetic and nonmagnetic layers) is considered, the resistance R^{AP} in the antiparallel alignment of magnetizations and the difference ΔR between the resistance of antiparallel alignment and that of parallel alignment R^P are, respectively, given by

$$R^{AP} = N(\rho_N^* t_N + \rho_F^* t_F + 2r_b^*), \tag{7}$$

$$\Delta R = R^{AP} - R^P = N^2(\beta\rho_F^* t_F + 2\gamma r_b^*)^2/R_{AP}. \quad (8)$$

Alternatively, these equations can be written as

$$\left(\frac{\Delta R}{R^{AP}}\right)^{-1/2} = \frac{\rho_F^* t_F + 2r_b^*}{\beta\rho_F^* t_F + 2\gamma r_b^*} + \frac{\rho_N^* t_N}{\beta\rho_F^* t_F + 2\gamma r_b^*}. \quad (9)$$

The above expression shows that $(\Delta R/R^{AP})^{-1/2}$ varies linearly with the nonmagnetic layer thickness t_N. Most experimental data obtained for CPP-GMR have been interpreted using the series-resistor model. The series-resistor model is generally a better approximation to explain the CPP-GMR than the CIP-GMR,[24] assuming that there is no spin-flipping effect between the two spin channels. The series-resistor model is applicable when spin-flipping is negligible when the thicknesses of both the magnetic and nonmagnetic layers are much smaller than the spin diffusion lengths for the metals in the layers. The concept of spin diffusion length was introduced in the Valet-Fert model of CPP-GMR.[19,20] The spin diffusion length l_{sf} represents the distance over which Mott's two-current model is valid. According to the Valet-Fert model, both the resistance R^P for the parallel alignment of magnetizations and the resistance R^{AP} for the antiparallel alignment of magnetizations depend on the spin diffusion length l_{sf}^N of the nonmagnetic layers and the length l_{sf}^F for the magnetic layers. Basically the Valet-Fert model is applicable to multilayers with any layer thicknesses. General expressions for R^{AP} and R^P derived in the Valet-Fert model are given in Ref. 19. We discuss our results using the Valet-Fert model.

The Valet-Fert model has provided three important conclusions.[25] First, when $t_N \ll l_{sf}^N$ and $t_F \ll l_{sf}^F$, the model leads to the series-resistor model described above. Second, when $t_N \gg l_{sf}^N$ and $t_F \ll l_{sf}^F$, the MR change is expected to decrease with increasing t_N in the form of $\exp(-t_N/l_{sf}^N)$. Thirdly, when $t_N \ll l_{sf}^N$ and $t_F \gg l_{sf}^F$, the CPP-GMR is inversely-proportional to t_F, that is

$$\frac{\Delta R}{R^P} = \frac{2p\beta^2 l_{sf}^F}{(1-\beta^2)t_F}, \quad (10)$$

where p is the fraction of consecutive magnetic layers that have magnetizations aligned antiparallel. It should be noted that the spin-mixing effect associated with a spin-moment transfer between the two spin channels by spin-flipping electron-magnon scattering has not been considered in Eqs. (9) and (10). The spin-mixing effect has been introduced in the Valet-Fert model.[26] However, as shown in Ref. 27, the spin-mixing effect does not make much difference in extracting parameters such as β from Eqs. (9) and (10) since the resistivity due to the spin-mixing effect is much smaller than the renormalized resistivity ρ_F^* at any temperature including room temperature. Hence in the qualitative discussion of the CPP-GMR data obtained for CoNi/Cu multilayer nanowires, the spin-mixing effect can be neglected when Eqs. (9) and (10) are used to explain the data. Also, it is difficult to rigorously determine all these parameters from experimental data, however it is possible to qualitatively estimate some of these parameters.

According to the Valet-Fert model in the long spin diffusion limit or the series-resistor model, $(\Delta R/R^{AP})^{-1/2}$ varies linearly with the nonmagnetic layer thickness t_N as given by Eq. (9). We evaluated our data by plotting $(\Delta R/R^{AP})^{-1/2}$ as a function of t_{Cu} as shown in Fig. 4(b) to assess whether the experimental data agree with the theoretically estimated values and indeed we found a good agreement between them. The fitting curve obtained from Eq. (9) is in the form of

$$\left(\frac{\Delta R}{R^{AP}}\right)^{-1/2} = a \cdot t_{Cu} + b, \quad (11)$$

where $a = \frac{\rho_N^*}{\beta\rho_F^* t_F + 2\gamma r_b^*}$ and $b = \frac{\rho_F^* t_F + 2r_b^*}{\beta\rho_F^* t_F + 2\gamma r_b^*}$. Using the data given in Fig. 4(b), we obtained $a = 0.21 \pm 0.01$ and $b = 1.31 \pm 0.23$.

As shown in Eq. (10) in the limit of $t_N \ll l_N$ and $t_F \gg l_F$, $(\Delta R/R^P)^{-1}$ is proportional to t_F and can be described as

$$\left(\frac{\Delta R}{R^P}\right)^{-1} = ct_F, \quad (12)$$

where $c = \frac{1-\beta^2}{2p\beta^2 l_{sf}^F}$. To obtain a better fitting of the Valet-Fert model given in Eq. (10) to our experiment data, we chose the value of t_{CoNi} in the range 30–170 nm, see Fig. 6(b). In this condition, t_{CoNi} is larger than the spin diffusion length l_{sf}^F for CoNi, and the contribution from AMR is probably negligible compared to the contribution from GMR. The best fitting yields $c = 0.42 \pm 0.03$. The linear variation agrees with the trend predicted from Eq. (10). This agreement also indicates that the value of p is constant in this range of t_{CoNi}; any CoNi/Cu multilayer samples with t_{CoNi} in this range would have the same fraction of magnetizations aligned antiparallel to each other between successive magnetic layers when the MR is at a maximum.

It is shown that the Cu layer thickness t_{Cu} dependence of CPP-GMR for $t_{CoNi} = 10.4$ nm and $t_{Cu} = 4.2$–42 nm can be consistently explained using the Valet-Fert model when the spin diffusion length is sufficiently long. Hence it is reasonable to deduce that the spin diffusion length l_{sf}^F for CoNi is larger than t_{CoNi}(=10.4 nm), and the spin diffusion length l_{sf}^N for Cu is larger than $t_{Cu} = 42$ nm which is the maximum Cu layer thickness examined. According to the Valet-Fert model, the MR is expected to decrease exponentially with increasing t_{Cu} when $t_{Cu} > l_{sf}^N$.

To gain further insights into the spin transport mechanism in CPP-GMR, we define an additional parameter g which represents the ratio of the interfacial resistance to the bulk resistance for CoNi layers. The parameter g is defined by

$$g = \frac{2r_b^*}{\rho_F^* t_F} = \frac{1 - b\beta}{b\gamma - 1}, \quad (13)$$

where the parameter γ is described in terms of β and g as

$$\gamma = \frac{1 + g - 1.31\beta}{1.31g}. \quad (14)$$

As shown in Eq. (12), $(\Delta R/R^P)^{-1}$ is proportional to t_F for multilayers with $t_F = 34$–170 nm and $t_N = 4.2$ nm and dependent on l_{sf}^F, p, and β besides t_F. The linear dependence of $(\Delta R/R^P)^{-1}$ on t_F shows that p is approximately constant in

this range of t_F. When t_N is small, the dipole-dipole interaction between neighboring magnetic layers may not be negligible. In this case, the interaction tends to align the magnetizations of successive magnetic layers antiparallel to minimize the magnetostatic energy so that the value of p increases and approaches unity when they become perfectly antiparallel. In the real system, it is likely to have $p<1$. More detailed discussion on the effects of the dipolar interlayer coupling on the CPP-GMR in CoNi/Cu nanowires is described later.

To estimate the values of β and γ, it is probably reasonable to assume that $p=0.75$ which represents the intermediate state between the perfectly antiparallel alignment ($p=1$) and a completely random alignment ($p=0.5$). When the spin-mixing effect is not considered and $p=0.75$ for Eq. (12), one obtains $\beta<0.37$ for the bulk spin asymmetry coefficient of CoNi since l_{sf}^{F} is greater than 10 nm. Also, since $g>0$, γ has to be greater than $1/b(=0.76)$. Hence it is inferred that $\beta \ll \gamma$. Indeed, the same relationship has been previously reported for the CPP-GMR of Co/Cu multilayers measured at low temperatures.[28–32] Various Co/Cu multilayer thin films[28–30] and nanowires[31,32] prepared using different fabrication methods have been studied and found to give quite different values of the bulk resistivity of the layers. The observed variation of the bulk resistivity, which may be due to the different defect densities in the samples can lead to a variation of the spin-asymmetry scattering parameters β and γ. However, $\gamma>\beta$ for bulk Co which is essentially independent of the fabrication method. It is inferred that the spin-dependent interfacial scattering plays an important role in determining the CPP-GMR effect in multilayers. According to Eq. (9), the bulk resistance becomes comparable to the interfacial resistance when $t_F=2\gamma r_b^*/\beta\rho_F^*=g\gamma/\beta$. Since $\beta<0.37$ and $\gamma<1$, it indicates from Eq. (13) that $g>1.66$. When the bulk resistance has a larger contribution to the CPP-GMR than the interfacial resistance, it indicates that $t_{\mathrm{CoNi}}>36$ nm assuming $\gamma=0.8$. Hence, when the magnetic layers have a thickness of a few nanometers, the dominant contribution to the CPP-GMR is the spin-dependent interfacial resistance.

B. Effect of dipole-dipole interactions between magnetic layers on CPP-GMR

Among various methods available to characterize magnetic properties of materials, magnetoresistance (MR) measurement has several advantages over other methods such as vibrating sample magnetometry (VSM) and SQUID. For example, the MR measurement does not strongly depend on the magnetization of the sample, because for MR the resistance of the sample is measured, whereas for VSM and SQUID, the magnetic moment is measured, requiring that the magnetic moment of the sample should be larger than the detection limit of the VSM or SQUID. In the case of CoNi/Cu nanowires, their magnetization may be very weak when t_{CoNi} is very small. Also, magnetic moment measurement techniques are mostly designed to probe the magnetization of an entire sample. In contrast, it is possible to measure the magnetic behavior of individual nanowires by MR measurement.

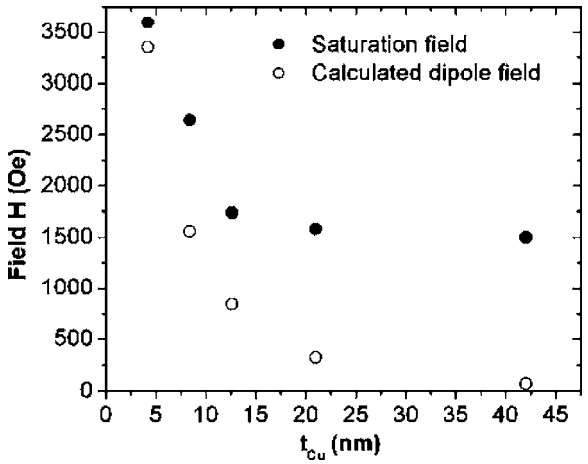

FIG. 7. Saturation fields (filled circles) extracted from the MR curves obtained for CoNi/Cu nanowire when $t_{\mathrm{CoNi}}=10.2$ nm and $t_{\mathrm{Cu}}=4.2$ nm, 8.4 nm, 12.6 nm, 21 nm, and 42 nm. The open circles shown in the graph are estimated dipole-dipole interaction fields exerted between neighboring CoNi layers in each nanowire.

Indeed, the MR data obtained for CoNi/Cu nanowires shown in Fig. 3 can be utilized to gain insights into their magnetic behavior. Figure 7 shows that the saturation field H_{sat} of CoNi/Cu nanowires tends to decrease with increasing t_{Cu} probably due to the decreasing dipole-dipole interaction between the adjacent CoNi layers. When the CoNi layers are in a thin disk shape, the dipolar interlayer coupling tends to align the magnetizations of adjacent CoNi layers antiparallel to each other.[33,34] Since t_{Cu} is in the range 4.2–42 nm, RKKY-type exchange interlayer coupling[35–37] should be negligibly small. However, the dipolar interlayer coupling may not be negligible and induces antiparallel alignment of magnetizations in the magnetic layers. In this case, some of the CoNi layers have magnetizations oriented differently and produce magnetostatic stray fields around the neighboring magnetic layers so that the effective magnetic field is reduced. When a magnetic field is applied perpendicular to the nanowire axis (i.e., parallel to the CoNi layers), magnetization reversal occurs when the applied field exceeds the magnetostatic field H_{dipo} associated with the dipolar interlayer coupling. When the dipolar interlayer coupling prevails, H_{sat} increases. When each magnetic layer is approximated to be a dipole, $H_{\mathrm{dipo}}=m/4\pi(t_{\mathrm{Cu}}+t_{\mathrm{CoNi}})^3$, where m is the magnetic moment of each magnetic layer. Apparently, H_{dipo} decreases with increasing t_{Cu}. The Cu layer thickness t_{Cu} dependence of H_{dipo} estimated for CoNi/Cu nanowires with $t_{\mathrm{CoNi}}=10.2$ nm is shown in Fig. 7. With increasing t_{Cu} from 4.2 nm to 42 nm, H_{dipo} decreases from 3350 Oe to 70 Oe. It is obvious in Fig. 7 that the measured values of H_{sat} are larger than the calculated values of H_{dipo} for all t_{Cu} and nearly constant when $t_{\mathrm{Cu}}>21$ nm. The finite values of H_{sat} are probably due to the dipolar interlayer coupling, but some other factors such as hindered domain wall motion during magnetization reversal may also contribute to the increase of H_{sat}. If the dipolar interlayer coupling is the only factor to increase H_{sat} for CoNi/Cu nanowires, H_{sat} would approach zero when $t_{\mathrm{Cu}}>21$ nm, see Fig. 7.

With increasing t_{Cu}, both the dipolar interlayer coupling and the MR decrease, as shown in the linear variation

of $(\Delta R/R^{AP})^{-1/2}$ with t_{Cu} for $t_{Cu}=4.2-42$ nm. In permalloy(Py)/Cu nanowires, Dubois[38] has found that a linear dependence of $(\Delta R/R^{AP})^{-1/2}$ on t_{Cu} in Py/Cu nanowires can be observed only when the permalloy layers are thin (a few nanometers) and the Cu layers are thick, e.g., $t_{Py}=4$ nm and $t_{Cu}>20$ nm. With increasing t_{Cu}, the dipolar interlayer coupling decreases so that the magnetization of the Py layers can be aligned more randomly (or p decreases). In the case of CoNi/Cu nanowires with thin disk-shaped CoNi layers, the dipolar interlayer coupling does not cause a significant deviation from the relationship represented by Eq. (9). Hence, the dipolar interlayer coupling may not have a significant effect on the MR but can modify the sharpness of the MR curve by changing H_{sat}.

The effect of dipolar interlayer coupling on CPP-GMR in CoNi/Cu nanowires also depends on t_{CoNi}. As shown above for CoNi/Cu nanowires with thin disk-shaped CoNi layers, the dipolar interlayer coupling can induce an antiparallel alignment of magnetizations between the CoNi layers. In contrast, the dipolar interlayer coupling in CoNi/Cu nanowires with thick rod-shaped CoNi layers tends to align their magnetizations parallel to each other in the direction along the nanowire axis. Since a linear dependence of GMR on $1/t_{CoNi}$ is observed in Fig. 6, it is reasonable to expect a constant value of p for various t_{CoNi}. However, Dubois *et al.* obtained a different result for Py/Cu nanowires with the diameter of 90 nm. Indeed, they observed that the GMR was not inversely proportional to t_{Py} in the range of t_{Py} they studied.[38] They attributed the observed deviation to a decrease in the parameter p for Py/Cu nanowires with thick permalloy layers and thin Cu layers. To explain the difference between our results for CoNi/Cu and Dubois's results for Py/Cu, the difference in the diameter of the nanowires should be considered. The diameter of our CoNi/Cu nanowires is about 250 nm, while that of Py/Cu nanowires is 90 nm. When nanowires of the exact same layer thicknesses are compared, the aspect ratio (layer thickness/wire diameter) of the layers in CoNi/Cu would be smaller than that of Py/Cu. Hence in the case of CoNi/Cu nanowires, the observed linear dependence of GMR on $1/t_{CoNi}$ when $t_{CoNi}=34-170$ nm suggests that the parameter p is approximately constant in this thickness range.

C. Superparamagnetic effect on CPP-GMR in ultrathin magnetic layers

Theoretical models typically assume an ideal and simplified case or a perfectly-layered multilayer structure. However, real multilayer samples often contain structural imperfections such as interfacial roughness and defects. For example, when magnetic layers are very thin, they may break into isolated segments or islands due to the interfacial roughness or nonuniformity of the layer thickness. The volume of individual islands may be so small that they exhibit a superparamagnetic behavior at room temperature, which would not be observed when the multilayer has a perfectly layered structure.[39] For example, the existence of structural imperfection in a multilayer is inferred in the MR data shown in Fig. 8 for CoNi/Cu nanowires with $t_{CoNi}=2$ nm. The MR curve is not saturated up to 9 kOe in this case, which is probably due to the presence of fragmented magnetic layers that exhibit superparamagnetism. Because the magnetic segments are likely to have a size distribution within the sample, smaller segments may be superparamagnetic (SPM) and larger ones may be ferromagnetic (FM). In this case, the MR data would indeed reflect both FM and SPM contributions. The superparamagnetic behavior of small magnetic elements can be described by the Langevin function $L(\alpha)=\coth(\alpha)-1/\alpha$, where $\alpha=\mu H/kT$, μ is the magnetic moment of a SPM element, k is the Boltzmann constant, and T is temperature. The saturation field H_{sat} for a SPM element is dependent greatly on its size and usually larger than H_{sat} for a FM element. It has been previously shown for the CIP-GMR of electrodeposited Co/Cu films[40–43] that the MR data actually represent both the contribution from the FM regions which is constant and that from the SPM regions which is field dependent when the data are obtained under magnetic fields H larger than H_{sat} for the FM regions. That is, for H larger than H_{sat}, the net MR is given by the sum of the ferromagnetic term MR_{FM} and the superparamagnetic term MR_{SPM} as

$$MR(H) = MR_{FM} + MR_{SPM}(H). \tag{15}$$

The SPM term can be described by the Langevin function, i.e., $MR_{SPM}(H)$ is proportional to $L(\alpha)$.

The MR data obtained for CoNi/Cu nanowires with $t_{Cu}=4.2$ nm and $t_{CoNi}=2$ nm can be evaluated using $H_{sat}=3$ kOe for the FM regions. To obtain $MR_{SPM}(H)$, the experimental data for $H>3$ kOe were fitted with the Langevin function $L(\alpha)$. Subsequently, $MR_{FM}(H)$ was obtained using Eq. (15) for the entire range of H, as shown in Fig. 8. This analysis indicates that the SPM elements in determining the CIP-GMR may be similar to that for the CPP-GMR.

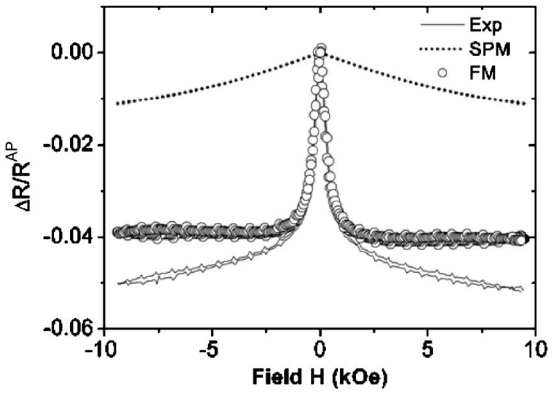

FIG. 8. Ferromagnetic (FM, open circles) and superparamagnetic (SPM, dotted line) contributions estimated from the experimentally obtained MR curve (solid thin line) for CoNi/Cu nanowires with $t_{Cu}=4.2$ nm and $t_{CoNi}=2$ nm. The experimental data for applied magnetic fields $H>3$ kOe are fitted using the Langevin function $L(\alpha)$ for the MR_{SPM} term where $\alpha=\mu H/kT$. The MR_{FM} term is obtained by subtracting the Langevin term $L(\alpha)$ from the experimental data in the entire range of applied magnetic fields.

V. CONCLUSIONS

We have measured the CPP-GMR of CoNi/Cu multilayer nanowires in a wide range of CoNi layer thickness and Cu

layer thickness, using a point contact method with a plunger tip. We have found that the number of nanowires used for the GMR measurements does not affect the measured GMR results, although care has to be taken when the number of nanowires is excessive or very few, where the contact resistance may not be negligible.

To explain the experiment CPP-GMR data obtained from the CoNi/Cu nanowires, the series-resistor model and the Valet-Fert model were utilized to discuss the transport mechanism. When both the Cu layer thickness t_{Cu} and CoNi layer thickness t_{CoNi} are much smaller than the spin diffusion length l of the corresponding materials, i.e., $t_{Cu} \ll l_{Cu}$ and $t_{CoNi} \ll l_{CoNi}$, $(\Delta R/R^{AP})^{-1/2}$ varies linearly to t_{Cu}. The obtained results agree well with the series-resistor model or the Valet-Fert model assuming that the spin diffusion length is sufficiently long. The experimental data and the theoretical models also show that, when $t_{Cu} \ll l_{Cu}$ and 170 nm $\gg t_{CoNi} \gg l_{CoNi}$, $(\Delta R/R^{P})^{-1}$ is proportional to t_{CoNi}. An analysis of the parameters in CPP-GMR shows that the interfacial spin asymmetry coefficient γ is much larger than the bulk spin asymmetry coefficient β, indicating that the interfacial scattering is important for the CPP-GMR. However, a deviation of the Valet-Fert model from the experimental data is observed when t_{CoNi} is very small, probably due to the existence of superparamagnetic layers. There is also a deviation from the experimental data for $t_{CoNi} > 170$ nm, where the contribution from anisotropic magnetoresistance (AMR) is not negligible.

ACKNOWLEDGMENT

The work was supported by the National Science Foundation Contract No. 05 06 738.

[1] M. N. Baibich, J. M. Broto, A. Fert, F. Nguyen Van Dau, F. Petroff, P. Etienne, G. Creuzet, A. Friederich, and J. Chazelas, Phys. Rev. Lett. **61**, 2472 (1988).
[2] D. A. Thompson and J. S. Best, IBM J. Res. Dev. **44**, 311 (2000).
[3] J. Bass and W. P. Pratt Jr., Physica B **321**, 1 (2002).
[4] W. P. Pratt, Jr., S.-F. Lee, J. M. Slaughter, R. Loloee, P. A. Schroeder, and J. Bass, Phys. Rev. Lett. **66**, 3060 (1991).
[5] M. A. Gijs, S. K. J. Lenczowski, R. J. M. van de Veerdonk, J. B. Giesbers, M. T. Johnson, and J. B. F. aan de Stegge, Phys. Rev. B **50**, 16733 (1994).
[6] M. A. Gijs, S. K. J. Lenczowski, and J. B. Giesbers, Phys. Rev. Lett. **70**, 3343 (1993).
[7] M. A. M. Gijs, Appl. Phys. Lett. **66**, 1839 (1995).
[8] A. Blondel, J. P. Meir, B. Doudin, and J.-Ph. Ansermet, Appl. Phys. Lett. **65**, 3020 (1994).
[9] K. Liu, K. Nagodawithana, P. C. Searson, and C. L. Chien, Phys. Rev. B **51**, 7381 (1995).
[10] L. Piraux, J. M. George, J. F. Despres, C. Leroy, E. Ferain, R. Legras, K. Ounadjela, and A. Fert, Appl. Phys. Lett. **65**, 2484 (1994).
[11] X.-T. Tang, G.-C. Wang, and M. Shima, J. Appl. Phys. **99**, 033906 (2006).
[12] J.-E. Wegrowe, S. E. Gilbert, V. Scarani, D. Kelly, B. Doudin, and J.-Ph. Ansermet, IEEE Trans. Magn. **34**, 903 (1998).
[13] F. Elhoussine, L. Vila, L. Piraux, and G. Faini, J. Magn. Magn. Mater. **290**, 116 (2005).
[14] K. Bouzehouane, V. Cros, C. Deranlot, and J.-M. George, Nanotechnology **16**, 2936 (2005).
[15] D. M. Edwards, J. Mathon, and R. B. Muniz, IEEE Trans. Magn. **3**, 3548 (1991).
[16] J. Mathon, Contemp. Phys. **32**, 143 (1991).
[17] N. F. Mott, Proc. R. Soc. London, Ser. A **156**, 368 (1936); N. F. Mott, Adv. Phys. **13**, 325 (1964).
[18] S. F. Lee, W. P. Pratt, R. Loloee, P. A. Schroeder, and J. Bass, Phys. Rev. B **46**, 548 (1992).
[19] T. Valet and A. Fert, Phys. Rev. B **48**, 7099 (1993).
[20] A. Fert, T. Valet, and J. Barnas, J. Appl. Phys. **75**, 6693 (1994).
[21] H. Schwanbeck and U. Schmidt, Electrochim. Acta **45**, 4389 (2000).
[22] X.-T. Tang, G.-C. Wang, and M. Shima, J. Magn. Magn. Mater. **309**, 188 (2006).
[23] B. Voegeli, A. Blondel, B. Doudin, and J.-Ph. Ansermet, J. Magn. Magn. Mater. **151**, 388 (1995).
[24] E. Y. Tsymbal and D. G. Pettifor, in *Solid State Physics*, edited by H. Ehrenreich and F. Spaepen (Academic Press, San Diego, 2001), Vol. 56, pp. 113–237.
[25] A. Fert and L. Piraux, J. Magn. Magn. Mater. **200**, 338 (1999).
[26] A. Fert, J. L. Duvail, and T. Valet, Phys. Rev. B **52**, 6513 (1995).
[27] L. Piraux, S. Dubois, A. Fert, and L. Belliard, Eur. Phys. J. B **4**, 413 (1998).
[28] J. Bass and W. P. Pratt Jr., J. Magn. Magn. Mater. **200**, 274 (1999).
[29] W. Oepts, M. A. M. Gijs, A. Reinders, R. M. Jungblut, R. M. J. van Gansewinkel, and W. J. M. de Jonge, Phys. Rev. B **53**, 14024 (1996).
[30] N. J. List, W. P. Pratt, M. A. Howson, J. Xu, M. J. Walker, and D. Greig, J. Magn. Magn. Mater. **148**, 342 (1995).
[31] L. Piraux, S. Dubois, and A. Fert, J. Magn. Magn. Mater. **159**, L287 (1996).
[32] B. Doudin, A. Blondel, and J.-Ph. Ansermet, J. Appl. Phys. **79**, 6090 (1996).
[33] M. Chen, P. C. Searson, and C. L. Chien, J. Appl. Phys. **93**, 8253 (2003).
[34] S. Dubois, C. Marchal, J. M. Beuken, L. Piraux, J. L. Duvail, A. Fert, J. M. George, and J. L. Maurice, Appl. Phys. Lett. **70**, 396 (1997).
[35] M. A. Ruderman and C. Kittel, Phys. Rev. **96**, 99 (1954).
[36] T. Kasuya, Prog. Theor. Phys. **16**, 4558 (1956).
[37] I. Yosida, Phys. Rev. **106**, 893 (1957).
[38] S. Dubois, L. Piraux, J. M. George, K. Ounadjela, J. L. Duvail, and A. Fert, Phys. Rev. B **60**, 477 (1999).
[39] X.-T. Tang, G.-C. Wang, and M. Shima, J. Appl. Phys. **99**, 123910 (2006).
[40] I. Bakonyi, L. Péter, Z. Rolik, K. Kiss-Szabó, Z. Kupay, J. Tóth, L. F. Kiss, and J. Pádár, Phys. Rev. B **70**, 054427 (2004).
[41] I. Bakonyi, L. Péter, V. Weihnacht, J. Tóth, L. F. Kiss, and C. M. Schneider, J. Optoelectron. Adv. Mater. **7**, 589 (2005).
[42] Qun-Xian Liu, László Péter, József Pádár, and Imre Bakonyi, J. Electrochem. Soc. **152**, C316 (2005).
[43] L. Péter, Z. Rolik, L. F. Kiss, J. Tóth, V. Weihnacht, C. M. Schneider, and I. Bakonyi, Phys. Rev. B **73**, 174410 (2006).